Preprints (www.preprints.org) | NOT PEER-REVIEWED | Posted: 12 April 2017 doi:10.20944/preprints201704.0066.v1

Peer-reviewed version available at Appl. Sci. 2017, 7, , 393; doi:10.3390/app7040393

Article

Modeling and Dynamics of a MDOF Isolation System

Youshuo Song and Xiuting Sun *

University of Shanghai for Science and Technology

* Correspondence: sunxiuting@usst.edu.cn; Tel.: +85-15000954547

Abstract: This study analyzes the modeling and dynamics of a novel passive in Multi-Degree-of-Freedom (MDOF) vibration isolation platform which can achieve significant isolation effect. Symmetrical Scissor-Like structures (SLSs) are utilized in the proposed MDOF isolation platform as the supporting and isolation elastic components. Based on the mathematical modeling and theoretical analysis of the MDOF vibration isolation system with SLSs, the effect of structural parameter and joint friction on stiffness and damping properties is investigated. It is shown that due to geometric relations within the SLSs, the natural frequencies can be reduced via adjusting structural parameters of the SLS for different direction vibration isolation. Theoretical and experimental results show that the SLS isolation platform can achieve much better loading capacity and vibration isolation performance simultaneously by only using linear passive components because of the MDOF adjustable stiffness property. Therefore, with low costing and energy consumption, the proposed novel isolation platform can provide the improvement of vibration suppression in various engineering practices.

Keywords: MDOF isolation platform; geometrical nonlinearity; vibration suppression, adjustable stiffness property

1. Introduction

It is required high stability and significant isolation performance for isolation system because it isolates the vibration to protect the instruments and equipment for many vibration environments. For different applications, different structures and control methods are carried out for different vibration suppression mechanisms, for example, energy transferring between different vibration modes [1-2], vibration suppressing with absorbers [3-5], or utilizing semi-active/active vibration control methods etc. [6-8]. In most cases in vibration isolation, better isolation effectiveness can be obtained by using elements with smaller restoring forces which result in smaller natural frequency of the system, especially for microgravity environment in aerospace engineering [9-11].

For various vibration isolation purposes, Quasi-zero-stiffness (QZS) vibration isolation systems for one direction vibration have been extensively studied to improve working environment and provide better background for aerospace devices and precision instruments [12-20]. In order to induce adjustable stiffness property with sufficient loading capacity, a structure with springs called Scissor-Like structure (SLS) is proposed. The most obvious advantage of the vibration isolation system with SLSs is that the natural frequency and nonlinear stiffness coefficients are dependent on the structural parameters, which could realize high static and low dynamic property. Considering the advantages of the structure with SLSs, the SLSs are utilized to construct a novel MDOF vibration isolation system. The proposed isolation system has nonlinear stiffness and damping characteristics in six directions, which are all adjustable and can achieve superior vibration isolation using only pure linear and passive elements in the system with a simple and flexible installation structure.

In the literature, the techniques of vibration isolation for multi-direction excitation with excellent isolation performance over larger frequency region have always been a hot and hard research topic. For the MDOF vibration isolation platform, active controllers are the chief method [9-11, 21-27]. The key point of the mechanism of active control in MDOF isolator is to generate anti-vibration forces in different directions by actuators and sensors in the designed system. The researches of MDOF isolation system are focused on the controllers and control strategies. Different

Preprints (www.preprints.org) | NOT PEER-REVIEWED | Posted: 12 April 2017 doi:10.20944/preprints201704.0066.v1

Peer-reviewed version available at Appl. Sci. 2017, 7, , 393; doi:10.3390/app7040393

designs and the analysis of the dynamics of parallel mechanism are studied [21-27], for example, hybrid magnet consisting of electromagnet and permanent magnets is used as the active actuators in Refs. 21 and 22. Although active controllers can actively isolate vibration and timely control vibration, considering the energy required by active actuators, passive isolation techniques provide higher stability without any external power [28].

This paper proposed a MDOF isolation platform using SLSs as the elastic components. Then the natural frequencies and vibration responses are studied to show the isolation effectiveness of the proposed system. The superior vibration isolation can be achieved using only pure linear and passive elements in the system with a simple and flexible installation structure because of the adjustable stiffness. This system could provide an effective solution to many engineering problems for excellent MDOF vibration suppression and sustainable development for microgravity environment. The paper is organized as follows. The prototype of the isolation platform with SLSs is carried out and its mathematical modeling is obtained in Section 2. In Section 3, the responses of the isolation system obtained by Harmonic Balance Method (HBM) [28] and experiment are conducted, and the isolation effectiveness of the proposed isolation system is compared to the one using linear springs as isolator. A conclusion is drawn at the last section.

2. 2 The prototype and modeling of the proposed isolation platform

2.1 Experimental prototype

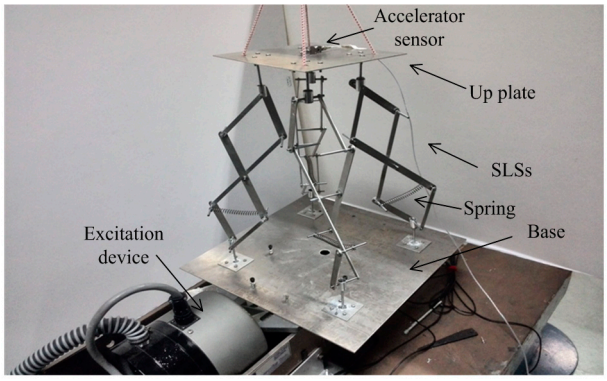

Figure 1. Experimental prototype of the MDOF isolation system with SLSs.

Figure 1 is the experimental prototype of the proposed MDOF isolation system with SLSs. As shown in Figure 1, the up plate of the isolation platform is connected with the base by four scissor-like structures (SLSs). The SLS is consisted of several connecting rods and a linear spring is assembled in one layer in each SLS.

2.2 Structural diagram

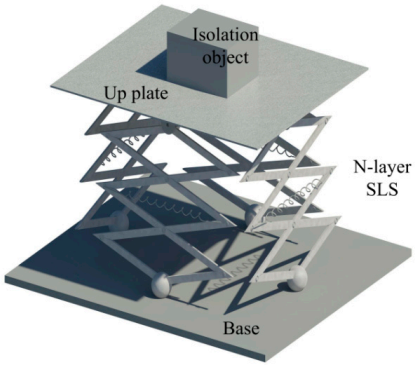

Figure 2. The structural diagram of the MDOF isolation system

Preprints (www.preprints.org) | NOT PEER-REVIEWED | Posted: 12 April 2017 doi:10.20944/preprints201704.0066.v1

Peer-reviewed version available at Appl. Sci. 2017, 7, , 393; doi:10.3390/app7040393

Figure 2 is the structural diagram of the isolation system. Considering the isolation platform is proposed for protecting an instrument (the isolation object) which is put on arbitrary position on the up plate, the location of the isolation object and the connecting point of the SLS are shown in Figure 3.

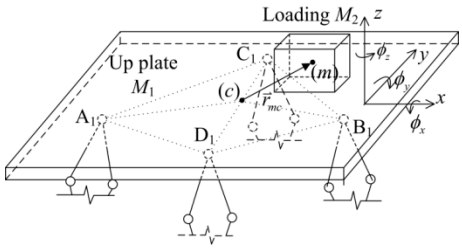

Figure 3. Geometry of the up plate and the isolation object M_2 and the coordinates.

In Figure 3, Point (c) is the geometrical and mass center of the up plate M_1 and Point (m) is the center of isolation object with mass M_2. The vector the origin of the up plate (c) and the isolation object (m) is as $\boldsymbol{r}_{mc}$={L_1, L_2, L_3}. The absolute motion of the platform $\boldsymbol{x}$={x, y, z, ϕ_x, ϕ_y, ϕ_z} are chosen as generalized coordinates.

2.3 *Modeling*

Lagrange principle is used to obtain the model of the isolation platform. The mass of connecting rods and joints in SLSs are neglected because their weights are much smaller compared to the up plate, base and isolation object. The kinetic energy consists of the up plate and the isolation object M_2, which are set as T_1 and T_2. The velocity of the up plate is the velocity at the center (c), thus the kinetic energy T_1 is as

$$T_1 = \frac{1}{2}M_1(\dot{x}^2 + \dot{y}^2 + \dot{z}^2) + \frac{1}{2}J_{xx}\dot{\phi}_x^2 + \frac{1}{2}J_{yy}\dot{\phi}_y^2 + \frac{1}{2}J_{zz}\dot{\phi}_z^2 \quad (1)$$

For the isolation object M_2 whose center has distance to the center of the center of the up plate, its velocity contains the translational velocity around Point (c) and the rotational velocity around the center Point (m). Figure 4 is the motions of the isolation object M_2 which represents the isolation object (e.g. precise instruments etc.).

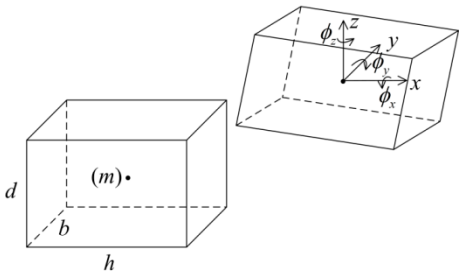

Figure 4. The motion of the object M_2 on the up plate.

Figure 4 is the deflections of the isolation object M_2 on the up plate whose moments of inertia in different rotational direction are defined as J_{xxm}, J_{yym} and J_{zzm}. Figure 5 is the deflection of one of the SLS in the isolator. From Figure 4, the kinetic energy T_2 of the isolation object is as

$$T_2 = \frac{1}{2}M_2\left[\left(\dot{x} + \dot{\phi}_y L_3 - \dot{\phi}_z L_2\right)^2 + \left(\dot{y} - \dot{\phi}_x L_3 + \dot{\phi}_z L_1\right)^2 + \left(\dot{z} + \dot{\phi}_x L_2 - \dot{\phi}_y L_1\right)^2\right]$$

$$+\frac{1}{2}J_{xxm}\dot{\phi}_x^2 + \frac{1}{2}J_{yym}\dot{\phi}_y^2 + \frac{1}{2}J_{zzm}\dot{\phi}_z^2 \quad (2)$$

Preprints (www.preprints.org) | NOT PEER-REVIEWED | Posted: 12 April 2017 doi:10.20944/preprints201704.0066.v1

Peer-reviewed version available at Appl. Sci. 2017, 7, , 393; doi:10.3390/app7040393

Therefore, the kinetic energy T of the system is as

$$T = T_1 + T_2 = \frac{1}{2}M_1(\dot{x}^2 + \dot{y}^2 + \dot{z}^2) + \frac{1}{2}J_{xx}\dot{\phi}_x^2 + \frac{1}{2}J_{yy}\dot{\phi}_y^2 + \frac{1}{2}J_{zz}\dot{\phi}_z^2 + \frac{1}{2}M_2\left[\left(\dot{x} + \dot{\phi}_y L_3 - \dot{\phi}_z L_2\right)^2 + \left(\dot{y} - \dot{\phi}_x L_3 + \dot{\phi}_z L_1\right)^2 + \left(\dot{z} + \dot{\phi}_x L_2 - \dot{\phi}_y L_1\right)^2\right] + \frac{1}{2}J_{xxm}\dot{\phi}_x^2 + \frac{1}{2}J_{yym}\dot{\phi}_y^2 + \frac{1}{2}J_{zzm}\dot{\phi}_z^2 \quad (3)$$

The potential energy V of the system is from the deformation of the springs in SLSs. The deflections of SLSs in the system are shown in Figure 5. The points connecting by SLS in the base are defined as A_0, B_0 and C_0; the points in the up plate are defined as A_1, B_1 and C_1; and the points in the up plate for deflection are defined as A'_1, B'_1 and C'_1.

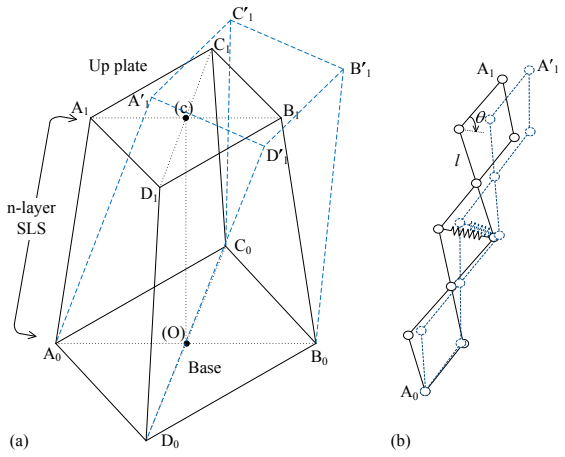

Figure 5. Deflection of the isolation system. (a) is the location of up plate and SLSs, and (b) is the deflection of one SLS.

Figure 5 is the deflections of the MDOF vibration isolation system and each SLS. From Figure 5 (a), it can be seen that the points A_0, B_0, C_0 and D_0 make a quadrilateral, and A_1, B_1, C_1 and D_1 are also make a quadrilateral. From Figure 5 (b) which is the deflection of the SLS, the original length of the springs in SLS is as $2l\cos\theta$, and the length of the springs can be obtained by $\|\mathbf{A}_0\mathbf{A}'_1\|$. Because the absolute motions of up plate at center $\boldsymbol{x}=\{x, y, z, \phi_x, \phi_y, \phi_z\}$ are chosen as generalized coordinate where x, y and z are the absolute translational motions and ϕ_x, ϕ_y and ϕ_z are absolute rotational motions, the location of point A'_1, B'_1 and C'_1 can be obtained by coordinate transformation matrix. Due to the six-excitation excitations from base which are as $\boldsymbol{x}_e=\{x_e, y_e, z_e, \phi_{xe}, \phi_{ye}, \phi_{ze}\}$, the relative motions of the up plate at center are as $\hat{\boldsymbol{x}}=\{\hat{x}, \hat{y}, \hat{z}, \hat{\phi}_x, \hat{\phi}_y, \hat{\phi}_z\}$. The transformation matrixes in the three rotational directions are as $\mathbf{R}_x$, $\mathbf{R}_y$ and $\mathbf{R}_z$, thus the rotational transformation matrix is defined as $\mathbf{R}$ which is dot product of the three transformation matrixes.

$$\mathbf{R} = \mathbf{R}_x \cdot \mathbf{R}_y \cdot \mathbf{R}_z = \begin{bmatrix} 1 & 0 & 0 \\ 0 & \cos\hat{\phi}_x & \sin\hat{\phi}_x \\ 0 & -\sin\hat{\phi}_x & \cos\hat{\phi}_x \end{bmatrix} \cdot \begin{bmatrix} \cos\hat{\phi}_y & 0 & -\sin\hat{\phi}_y \\ 0 & 1 & 0 \\ \sin\hat{\phi}_y & 0 & \cos\hat{\phi}_y \end{bmatrix} \cdot \begin{bmatrix} \cos\hat{\phi}_z & \sin\hat{\phi}_z & 0 \\ -\sin\hat{\phi}_z & \cos\hat{\phi}_z & 0 \\ 0 & 0 & 1 \end{bmatrix}$$
$$= \begin{bmatrix} \cos\hat{\phi}_y\cos\hat{\phi}_z & \cos\hat{\phi}_y\sin\hat{\phi}_z & -\sin\hat{\phi}_y \\ \sin\hat{\phi}_x\sin\hat{\phi}_y\cos\hat{\phi}_z - \cos\hat{\phi}_x\sin\hat{\phi}_z & \cos\hat{\phi}_x\cos\hat{\phi}_z + \sin\hat{\phi}_x\sin\hat{\phi}_y\sin\hat{\phi}_z & \sin\hat{\phi}_x\cos\hat{\phi}_y \\ \cos\hat{\phi}_x\sin\hat{\phi}_y\cos\hat{\phi}_z + \sin\hat{\phi}_x\sin\hat{\phi}_z & -\sin\hat{\phi}_x\cos\hat{\phi}_z + \cos\hat{\phi}_x\sin\hat{\phi}_y\sin\hat{\phi}_z & \cos\hat{\phi}_x\cos\hat{\phi}_y \end{bmatrix} \quad (4)$$

where $\mathbf{R}_x$, $\mathbf{R}_y$ and $\mathbf{R}_z$ are rotational transformation matrix in ϕ_x, ϕ_y and ϕ_z directions.

From Figure 5, assuming the coordinate of point (c) is {0, 0, 0}, for the generalization of the results, the vector $\mathbf{cA}_0$, $\mathbf{cB}_0$, $\mathbf{cC}_0$ and $\mathbf{cD}_0$ are assumed as $\mathbf{cA}_0=\{x_{a0}, y_{a0}, z_{a0}\}$, $\mathbf{cB}_0=\{x_{b0}, y_{b0}, z_{b0}\}$, $\mathbf{cC}_0=\{x_{c0}, y_{c0},$

Preprints (www.preprints.org) | NOT PEER-REVIEWED | Posted: 12 April 2017 doi:10.20944/preprints201704.0066.v1

Peer-reviewed version available at Appl. Sci. 2017, 7, , 393; doi:10.3390/app7040393

$z_{c0}\}$ and $\mathbf{cD}_0=\{x_{d0}, y_{d0}, z_{d0}\}$, and the vector $\mathbf{cA}_1$, $\mathbf{cB}_1$, $\mathbf{cC}_1$ and $\mathbf{cD}_1$ are assumed as $\mathbf{cA}_1=\{x_{a1}, y_{a1}, z_{a1}\}$, $\mathbf{cB}_1=\{x_{b1}, y_{b1}, z_{b1}\}$, $\mathbf{cC}_1=\{x_{c1}, y_{c1}, z_{c1}\}$ and $\mathbf{cD}_1=\{x_{d1}, y_{d1}, z_{d1}\}$. Therefore, the vector $\mathbf{A}_0\mathbf{A'}_1$, $\mathbf{B}_0\mathbf{B'}_1$, $\mathbf{C}_0\mathbf{C'}_1$ and $\mathbf{D}_0\mathbf{D'}_1$ can be obtained by the translational motion matrix and rotational transformation matrix as

$$\begin{cases} \mathbf{A}_0\mathbf{A}'_1 = \mathbf{cA}'_0 - \mathbf{cA}_0 = \{\hat{x},\hat{y},\hat{z}\} + \mathbf{R}\cdot\mathbf{cA}_1 - \mathbf{cA}_0 \\ \mathbf{B}_0\mathbf{B}'_1 = \mathbf{cB}'_0 - \mathbf{cB}_0 = \{\hat{x},\hat{y},\hat{z}\} + \mathbf{R}\cdot\mathbf{cB}_1 - \mathbf{cB}_0 \\ \mathbf{C}_0\mathbf{C}'_1 = \mathbf{cC}'_0 - \mathbf{cC}_0 = \{\hat{x},\hat{y},\hat{z}\} + \mathbf{R}\cdot\mathbf{cC}_1 - \mathbf{cC}_0 \\ \mathbf{D}_0\mathbf{D}'_1 = \mathbf{cD}'_0 - \mathbf{cD}_0 = \{\hat{x},\hat{y},\hat{z}\} + \mathbf{R}\cdot\mathbf{cD}_1 - \mathbf{cD}_0 \end{cases} \tag{5}$$

From Eq. (5), the deflection of the axis of SLS is obtained, and then the deformations of springs in SLS can be obtained by the analysis of the shape of SLS. Figure 6 is the deflection of one layer of the SLS.

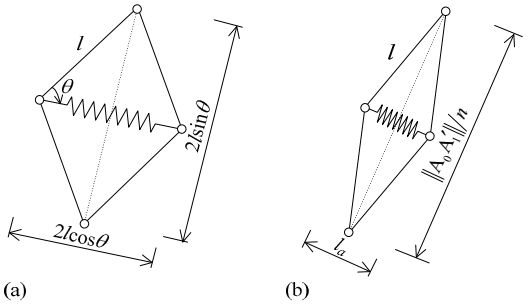

Figure 6. The deflection of one layer in the SLS. (a) is original shape, and (b) is deformed shape.

From Figure 6 (a), it can be seen that the original length of springs in the SLS is $2l\cos\theta$. For deflection, the lengths of the springs in the three SLS are defined as l_a, l_b, l_c and l_d which can be obtained by triangular relationship shown in Figure 6 (b) which is as

$$\begin{cases} l_a^2 + \left(\|\mathbf{A}_0\mathbf{A}'_1\|/n\right)^2 = 4l^2 \\ l_b^2 + \left(\|\mathbf{B}_0\mathbf{B}'_1\|/n\right)^2 = 4l^2 \\ l_c^2 + \left(\|\mathbf{C}_0\mathbf{C}'_1\|/n\right)^2 = 4l^2 \\ l_d^2 + \left(\|\mathbf{D}_0\mathbf{D}'_1\|/n\right)^2 = 4l^2 \end{cases} \tag{6}$$

The potential energy V of the system is consisted of the elastic energy of the four springs in SLSs which can be expressed as

$$\begin{aligned} V &= \frac{1}{2}k\left(l_a - 2l\cos\theta\right)^2 + \frac{1}{2}k\left(l_b - 2l\cos\theta\right)^2 + \frac{1}{2}k\left(l_c - 2l\cos\theta\right)^2 + \frac{1}{2}k\left(l_d - 2l\cos\theta\right)^2 \\ &= \frac{1}{2}k\left(\sqrt{4l^2 - \frac{\|\mathbf{A}_0\mathbf{A}'_1\|^2}{n^2}} - 2l\cos\theta\right)^2 + \frac{1}{2}k\left(\sqrt{4l^2 - \frac{\|\mathbf{B}_0\mathbf{B}'_1\|^2}{n^2}} - 2l\cos\theta\right)^2 \\ &\quad + \frac{1}{2}k\left(\sqrt{4l^2 - \frac{\|\mathbf{C}_0\mathbf{C}'_1\|^2}{n^2}} - 2l\cos\theta\right)^2 + \frac{1}{2}k\left(\sqrt{4l^2 - \frac{\|\mathbf{D}_0\mathbf{D}'_1\|^2}{n^2}} - 2l\cos\theta\right)^2 \end{aligned} \tag{7}$$

Considering the air damping of the system, the dynamic equation can be obtained by Lagrange principle as

$$\frac{d}{dt}\left[\frac{\partial(T-V)}{\partial\dot{\boldsymbol{x}}}\right] - \frac{\partial(T-V)}{\partial\boldsymbol{x}} = -\boldsymbol{C}\cdot\left(\dot{\boldsymbol{x}} - \dot{\boldsymbol{x}}_e\right) \tag{8}$$

Preprints (www.preprints.org) | NOT PEER-REVIEWED | Posted: 12 April 2017 doi:10.20944/preprints201704.0066.v1

Peer-reviewed version available at Appl. Sci. 2017, 7, , 393; doi:10.3390/app7040393

where T is the kinetic energy and V is the potential energy shown as Eq. (3) and Eq. (7), The mass matrix $\boldsymbol{M}$ of the system is as

$$\boldsymbol{M}=\begin{bmatrix} M_1+M_2 & 0 & 0 \\ 0 & M_1+M_2 & 0 \\ 0 & 0 & M_1+M_2 \\ 0 & -M_2L_3 & M_2L_2 \\ M_2L_3 & 0 & -M_2L_1 \\ -M_2L_2 & M_2L_1 & 0 \end{bmatrix}$$
$$\begin{bmatrix} 0 & M_2L_3 & -M_2L_2 \\ -M_2L_3 & 0 & M_2L_1 \\ M_2L_2 & -M_2L_1 & 0 \\ J_{xc}+J_{xm}+M_2\left(L_2^2+L_3^2\right) & -M_2L_1L_2 & -M_2L_1L_3 \\ -M_2L_1L_2 & J_{yc}+J_{ym}+M_2\left(L_1^2+L_3^2\right) & -M_2L_2L_3 \\ -M_2L_1L_3 & -M_2L_2L_3 & J_{zc}+J_{zm}+M_2\left(L_1^2+L_2^2\right) \end{bmatrix} \tag{9}$$

After first-order Taylor series expand, the stiffness matrix $\boldsymbol{K}$ is as

$$\boldsymbol{K}=\begin{bmatrix} \frac{k\left(l_2-l_1\right)^2}{2l^2n^4\cos^2\theta} & 0 & 0 & 0 & \frac{kl_1\left(l_1-l_2\right)H}{2l^2n^4\cos^2\theta} & 0 \\ 0 & \frac{k\left(l_2-l_1\right)^2}{2l^2n^4\cos^2\theta} & 0 & \frac{kl_1\left(l_2-l_1\right)H}{2l^2n^4\cos^2\theta} & 0 & 0 \\ 0 & 0 & \frac{kH^2}{l^2n^4\cos^2\theta} & 0 & 0 & 0 \\ 0 & \frac{kl_1\left(l_2-l_1\right)H}{2l^2n^4\cos^2\theta} & 0 & \frac{kl_1^2H^2}{2l^2n^4\cos^2\theta} & 0 & 0 \\ \frac{kl_1\left(l_1-l_2\right)H}{2l^2n^4\cos^2\theta} & 0 & 0 & 0 & \frac{kl_1^2H^2}{2l^2n^4\cos^2\theta} & 0 \\ 0 & 0 & 0 & 0 & 0 & 0 \end{bmatrix} \tag{10}$$

where $H=\sqrt{4n^2l^2\sin^2\theta-\left(l_2-l_1\right)^2}$, and matrix $\boldsymbol{C}$ is the damping matrix of the system as

$$\boldsymbol{C}=\begin{bmatrix} c_1 & & \cdots & & 0 \\ & c_2 & & & \\ & & c_3 & & \vdots \\ \vdots & & & c_4 & \\ & & & & c_5 \\ 0 & & \cdots & & c_6 \end{bmatrix} \tag{11}$$

where c_i (i=1,…,6) are damping coefficients in the six coordinates.

Because of the assumptions that the amplitudes of motions are sufficiently small, each term in the dynamic equation can be expanded by Taylor series and higher order terms can be neglected. Therefore, the dynamic equation of the system is as

$$\boldsymbol{M}\ddot{\boldsymbol{x}}+\boldsymbol{K}\boldsymbol{x}+\boldsymbol{C}\dot{\boldsymbol{x}}=\boldsymbol{K}\boldsymbol{x}_{\boldsymbol{e}}+\boldsymbol{C}\dot{\boldsymbol{x}}_{\boldsymbol{e}} \tag{12}$$

where $\boldsymbol{M}$ is the mass matrix, $\boldsymbol{K}$ is the stiffness matrix and $\boldsymbol{C}$ is the damping matrix, respectively, and $\boldsymbol{x}$ is the motion vector and $\boldsymbol{x}_e$ is the base excitation vector.

Preprints (www.preprints.org) | NOT PEER-REVIEWED | Posted: 12 April 2017 doi:10.20944/preprints201704.0066.v1

Peer-reviewed version available at Appl. Sci. 2017, 7, , 393; doi:10.3390/app7040393

3. Isolation effect

3.1. Solutions of system

The isolation effect of the proposed MDOF isolation platform with SLSs reflected by displacement transmissibility is based on the dynamic equation Eq. (12) and the responses for different structural parameters can be obtained by solving the linearized dynamic equations. When the excitation is harmonic excitation as $x_{ei}=e_i\cos\omega t$, the responses could be set as $x_i=a_i\cos(\omega t+\varphi)$. Then, the displacement transmissibility T_i (dB) could be defined as the ratio between the amplitude of response and the excitation in respective direction as

$$T_i = 10\log_{10}\left(\frac{|a_i|}{|e_i|}\right) \quad \left(i = x, y, z, \phi_x, \phi_y, \phi_z\right) \tag{13}$$

where a_i is the amplitude of response and e_i is the amplitude of harmonic excitation in different directions. From the dynamic equation Eq. (12) and mass, stiffness and damping matrices, it reveals that the values of components of the dynamic equations of each freedoms can be adjusted by changing the values of the structural parameters n, θ and l. The isolation effects for different structural parameters are shown in Figure 7.

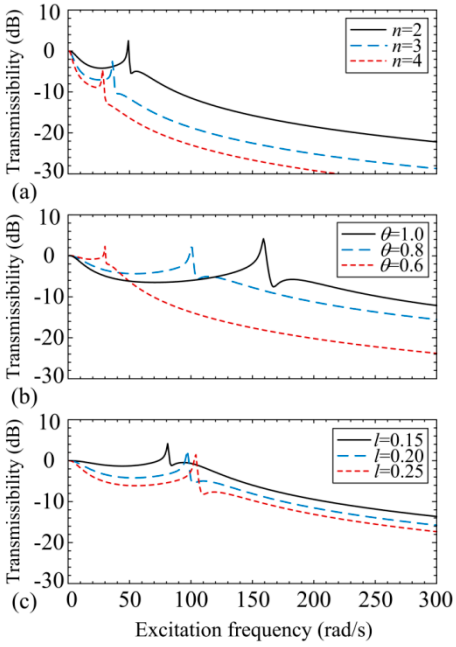

Figure 7. Isolation effect in x direction for different structural parameters (a) different n; (b) different θ; (c) different l.

From Figure 7, it can be seen that firstly the natural frequency where has largest peak is reduced by increasing n, or decreasing θ and l, which verifies the analysis of natural frequencies in pervious section. Secondly, the value of the peak is reduced by increasing n and l while changing θ has no obvious effect on the value of the peak, and thirdly the response of the amplitudes are lower for larger n and l, or smaller θ. Also, it demonstrates that the value of the displacement transmissibility (dB) in the frequency range from zero to the first resonant peak could be controlled less than zero and the displacement transmissibility is always below zero after the first resonant peak for larger n or l and smaller θ. Therefore, it can be concluded that the isolation effectiveness in a broad frequency

Preprints (www.preprints.org) | NOT PEER-REVIEWED | Posted: 12 April 2017 doi:10.20944/preprints201704.0066.v1

Peer-reviewed version available at Appl. Sci. 2017, 7, , 393; doi:10.3390/app7040393

band of the proposed isolation platform with SLSs can be improved by adjusting the structural parameters n, θ and l easily.

3.2. Comparison with normal spring-mass isolation platform

The isolation effectiveness of the isolation platform with SLSs and springs are compared which is shown in Figure 8. For two cases as n=2, $\theta=\pi/4$, l=0.2 (case 1) and n=3, $\theta=\pi/6$, l=0.2 (case 2), the performances of isolation platform with springs and SLSs are obtained and shown in Figure 8.

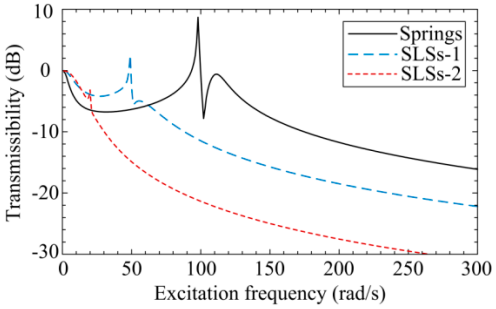

Figure 8. The comparison of the isolation effectiveness in x direction between the platform with springs and SLSs for n=2, $\theta=\pi/4$ and l=0.2 (case 1) and n=3, $\theta=\pi/6$ and l=0.2 (case 2).

From Figure 8, it can be seen that the isolation platform with springs has two obvious resonant peaks are about 100 and 110 rad·s^{-1} expect zero. While for the two cases of the isolation platform using SLSs, the fundamental natural frequency is much smaller than the one using springs. For case 1 as n=2, $\theta=\pi/4$ and l=0.2, the first resonant peak is at about 50 rad·s^{-1}, and for case 2 as n=3, $\theta=\pi/6$ and l=0.2, the first resonant peak is at 25 rad·s^{-1}. Also, the values of displacement transmissibility for the two cases of the platform with SLSs are much smaller than the case with springs in a broad frequency domain.

3.3 Isolation effectiveness

In order to obtain the natural frequency of the proposed MDOF isolation platform and its isolation effectiveness, random excitation is proposed on the base and the response of the experimental prototype. The frequency domain of the random excitation is from 0 to 100 Hz. The structural parameters of the experimental prototype are as n=2, l=0.1, l_2=0.285, l_1=0.105, M_2=0.22, M_1=0, L_1=L_2=L_3=0, and other structural parameters θ and k_1 could be adjusted easily for different isolation requirements. In Figure 9, two cases of isolation effectiveness are shown as θ and k_l are as $\theta=\pi/3$, k_l=900.

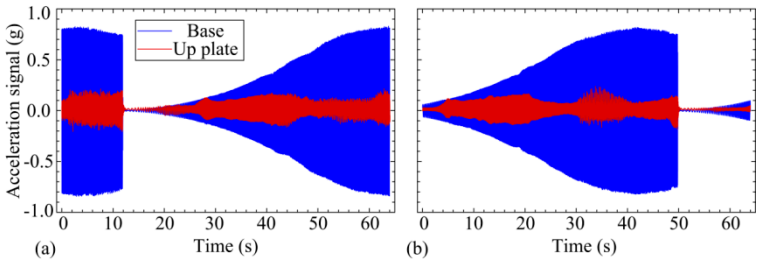

Figure 9. The isolation effectiveness for different structural parameters. (a) for $\theta=\pi/3$ and k_l=900; (b) $\theta=2\pi/5$ and k_l=450.

Figure 10 shows the comparison between the theoretical results and experimental results for

Preprints (www.preprints.org) | NOT PEER-REVIEWED | Posted: 12 April 2017 doi:10.20944/preprints201704.0066.v1

Peer-reviewed version available at Appl. Sci. 2017, 7, , 393; doi:10.3390/app7040393

the periodic excitation with z_e=0.03, x_e=y_e=ϕ_{xe}=ϕ_{ye}=ϕ_{ze}=0, θ=π/3 and k_l=900. The signals of the base and the up plate measured are acceleration signals and the acceleration signals are calculated to displacement signals by dividing the square of frequency since the vibrations are periodic motions.

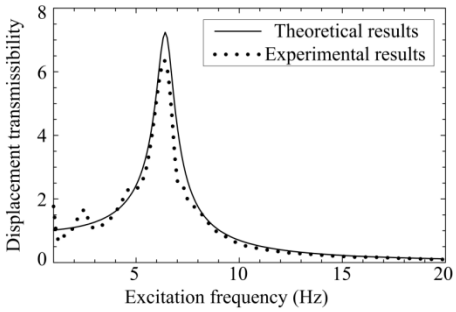

Figure 10. The displacement transmissibility for vertical direction vibration for θ=π/3, k_l=900 and z_e=0.03.

From Figure 10, the natural frequency of the proposed isolation platform could be reduced by adjusting the structural parameters of the SLSs for different structural parameters. When utilizing four springs with k_l=900 in a normal spring-damping isolator, the vertical-direction natural frequency is as $\sqrt{\frac{4\times900}{0.22}} = 128$ rad/s≈20.38 Hz, while for utilizing the SLSs the natural frequency could be reduced to about 6.4 Hz as shown in Figure 10 for θ=π/3, k_l=900. Therefore, using SLSs instead of springs could improve the isolation effectiveness, based on the fact that the natural frequency is reduced and the effective isolation range is increased.

4. Conclusions

This study proposed a MDOF vibration isolation platform with four symmetrical scissor-like structures (SLSs), which is designed for microgravity environments such as protecting instruments and isolation devices in aerospace stations. Theoretical modeling, analysis and comparison studies demonstrated its advantages and versatility in vibration isolation/control. The advantages of this isolation platform are listed as follow,

(a)By designing the structural parameters of SLSs, the proposed MDOF isolation platform can achieve smaller natural frequency and much larger effective isolation frequency range compared with normal spring-mass isolator;

(b)Because of the stiffness property with small linear coefficients in different directions of the proposed isolation platform, the system becomes an improved MDOF adjustable isolation platform;

(c)The adjustable stiffness coefficients in different directions and isolation effectiveness of the isolation platform with SLSs are verified by experiment prototype and experimental results.

Further studies will focus on the effect of active control for a MDOF vibration isolation system using the scissor-like structures (SLSs) and the combined effect of control parameters and nonlinear coefficients on isolation performance.

Preprints (www.preprints.org) | NOT PEER-REVIEWED | Posted: 12 April 2017 doi:10.20944/preprints201704.0066.v1

Peer-reviewed version available at Appl. Sci. 2017, 7, , 393; doi:10.3390/app7040393

Acknowledgments: The authors would like to gratefully acknowledge the support from a NSF projects (Ref 11602141) of China.

Author Contributions: Song Y.S. and Sun X.T. conceived and designed the experiments; Sun X.T. performed the experiments; Song Y.S. and Sun X.T. analyzed the data; Sun X.T. contributed reagents/materials/analysis tools; Song Y.S. wrote the paper.

Conflicts of Interest: The authors declare no conflict of interest. The founding sponsors had no role in the design of the study; in the collection, analyses, or interpretation of data; in the writing of the manuscript, and in the decision to publish the results.

References

1. Y.Y. Lee, R.K.L. Su, C.F. Ng, C.K. Hui, The Effect of Modal Energy Transfer on the Sound Radiation and Vibration of a Curved Panel: Theory and Experiment, Journal of Sound and Vibration 324 (2009) 103-1015.
2. A.M. Tusset, J.M. Balthazar, F.R. Chavarette, J.L. Pelix, On Energy Transfer Phenomena, in a Nonlinear Ideal and Nonideal Essential Vibrating Systems, Coupled to a (MR) MagnetoRheological Damper, Nonlinear Dynamics 69 (2012)1859-1880.
3. Y.Y. Zhao, J. Xu, Effects of delayed feedback control on nonlinear vibration absorber system. Journal of Sound and Vibration 308 (1-2) (2007) 212-230.
4. N. Jalili, D.W. Knowles IV, Structural vibration control using an active resonator absorber: modeling and control implementation. Smart Materials and Structures 13 (5) (2004) 998-1005.
5. R. Viguie, G. Kerschen, Nonlinear vibration absorber coupled to a nonlinear primary system: A tuning methodology. Journal of Sound and Vibration 326 (3-5) (2009) 780-793.
6. F. Casciati, J. Rodellar, U. Yildirim, Active and semi-active control of structures-theory and applications: A review of recent advances. Journal of Intelligent Material Systems and Structures 23 (11) (2012) 1181-1195.
7. H. Zhang, R.R. Wang, J.M. Wang, Y. Shi, Robust finite frequency H-infinity static-output-feedback control with application to vibration active control of structural systems. Mechatronics 24 (4) (2014) 354-366.
8. M.A. Beijen, D. Tjepkema, J. van Dijk, Two-sensor control in active vibration isolation using hard mounts. Control Engineering Practice 26 (2014) 82-90.
9. J.G. Liu, Y.M. Li, Y. Zhang, Q. Cao, B. Zuo, Dynamics and control of a parallel mechanism for active vibration isolation in space station. Nonlinear Dynamics 76 (3) (2014) 1737-1751.
10. C.M. Grodsinsky, M.S. Whorton, Survey of active vibration isolation systems for microgravity applications. Journal of Spacecraft and Rockets 37 (5) (2000) 586-596.
11. C.S. Mehendale, I.J. Fialho, K.M. Grigoriadis, A linear parameter-varying framework for adaptive active microgravity isolation. Journal of Vibration and Control 15 (5) (2009) 773-800.
12. I. Kovacic, M.J. Brennan, T.P. Waters, A study of a nonlinear vibration isolator with a quasi-zero stiffness characteristic. Journal of Sound and Vibration 315 (3) (2008) 700-711.
13. G. Gatti, I. Kovacic, M.J. Breenan, On the response of a harmonically excited two degree-of-freedom system consisting of a linear and a nonlinear quasi-zero stiffness oscillator. Journal of Sound and Vibration 329 (10) (2010) 1823-1835.
14. D.L. Xu, Y.Y. Zhang, J.X. Zhou, J.J. Lou, On the analytical and experimental assessment of the performance of a quasi-zero-stiffness isolator. Journal of Vibration and Control 20 (15) (2014) 2314-2325.
15. A. Carrella, M.J. Brennan, T.P. Waters, V. Lopes Jr, Force and displacement transmissibility of a nonlinear isolator with high-static-low-dynamic-stiffness. International Journal of Mechanical Sciences 55 (1) (2012) 22-29.
16. J.X. Zhou, D.L. Xu, S. Bishop, A torsion quasi-zero stiffness vibration isolator. Journal of Sound and Vibration 338 (2015) 121-133.
17. A.D. Shaw, S.A. Neild, D.J. Wagg, Dynamic analysis of high static low dynamic stiffness vibration isolation mounts. Journal of Sound and Vibration 332 (6) (2013) 1437-1455.
18. A. Carrella, M.I. Friswell, A. Zotov, D.J. Ewins, A. Tichonov, Using nonlinear springs to reduce the whirling of a rotating shaft. Mechanical Systems and Signal Processing 23 (7) (2009) 2228-2235.
19. X.T. Liu, X.C. Huang, H.X. Hua, On the characteristics of a quasi-zero stiffness isolator using Euler buckled beam as negative stiffness corrector. Journal of Sound and Vibration 332 (14) (2013) 3359-3376.
20. Z.F. Hao, Q.J. Cao, The isolation characteristics of an archetypal dynamical model with stable-quasi-zero-stiffness. Journal of Sound and Vibration 340 (2015) 61-79.

Preprints (www.preprints.org) | NOT PEER-REVIEWED | Posted: 12 April 2017 doi:10.20944/preprints201704.0066.v1

Peer-reviewed version available at Appl. Sci. 2017, 7, , 393; doi:10.3390/app7040393

21. M.E. Hoque, T. Mizuno, Y. Ishino, M. Takasaki, A three-axis vibration isolation system using modified zero-power controller with parallel mechanism technique. Mechatronics 21 (2011) 1055-1062.
22. M.E. Hoque, T. Mizuno, Y. Ishino, M. Takasaki, A six-axis hybrid vibration isolation system using active zero-power control supported by passive support mechanism. Journal Sound and Vibration 329 (17) (2010) 3417-3430.
23. F. Kerber, S. Hurlebaus, B.M. Beadle, U. Stobener, Control concepts for an active vibration isolation system. Mechanical Systems and Signal Processing 21 (2007) 3042-3059.
24. B. Li, W. Zhao, Z.Q. Deng, Modeling and analysis of a multi-dimensional vibration isolator based on the parallel mechanism. Journal of Manufacturing Systems 31 (2012) 50-58.
25. A. Preumont, M. Horodinca, I. Romanescu I, D. de Marneffe, M. Avraam, A. Deraemaeker, et al., A six-axis single-stage active vibration isolator based on Stewart platform. Journal Sound and Vibration 300 (3-5) (2007) 644-661.
26. I.Z. Mat Darus, M.O. Tokhi, Soft computing-based active vibration control of a flexible structure. Engineering Applications of Artificial Intelligence 28 (2005)93-114.
27. Y. Yun, Y.M. Li, A general dynamics and control model of a class of multi-DOF manipulators for active vibration control. Mechanism and Machine Theory 46 (2011) 1549-1574.
28. R.A. Ibrahim, Recent advances in nonlinear passive vibration isolators. Journal of Sound of Vibration 314 (3-5) (2008) 371-452.
29. A. H. Nayfeh, D. T. Mook, Nonlinear Oscillations, New York: Wiley-Interscience, 1979.

© 2017 by the authors. Licensee *Preprints*, Basel, Switzerland. This article is an open access article distributed under the terms and conditions of the Creative Commons by Attribution (CC-BY) license (http://creativecommons.org/licenses/by/4.0/).